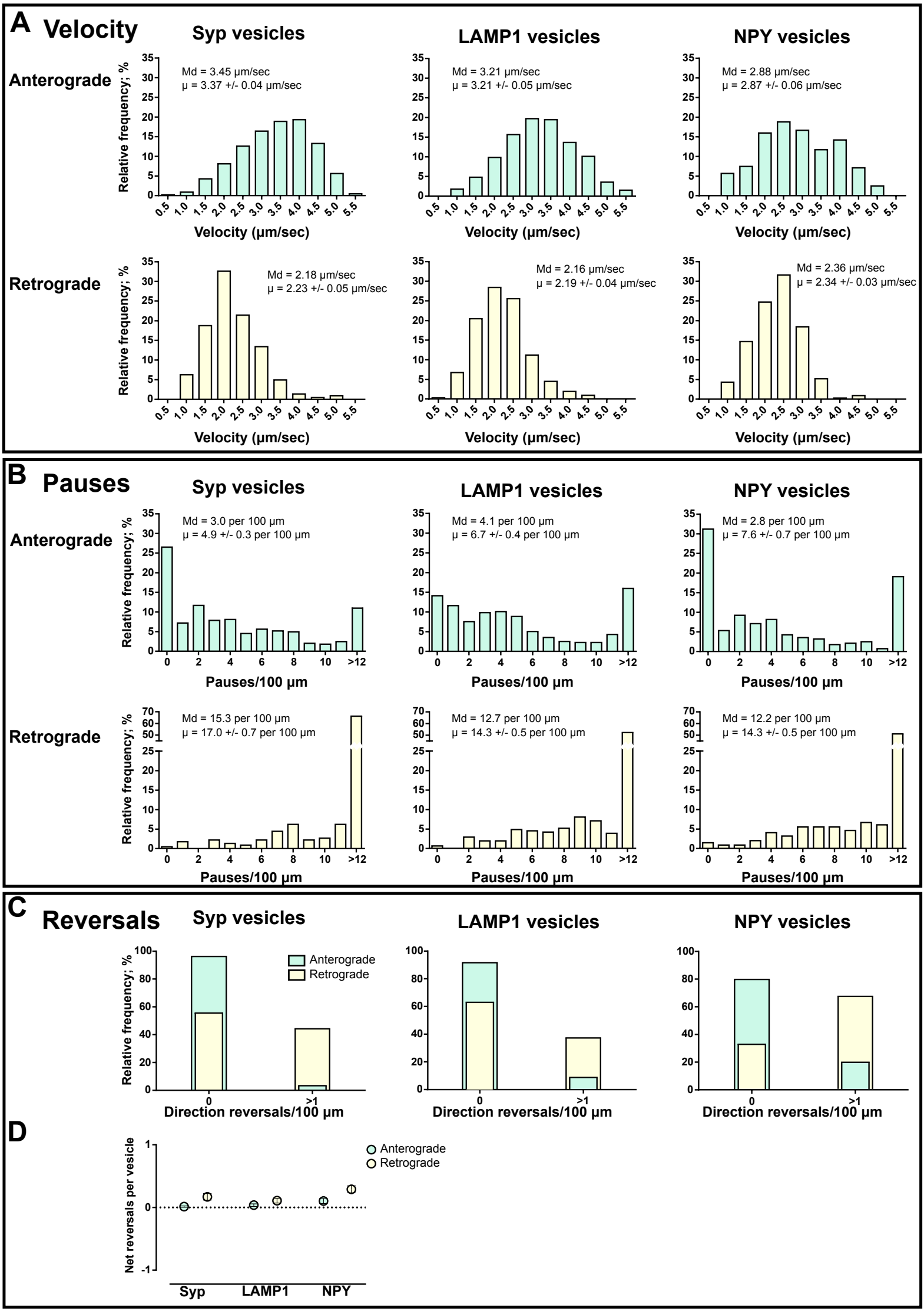
A Velocity
Syp vesicles
LAMP1 vesicles
NPY vesicles
Anterograde
Retrograde
Relative frequency; %
Md = 3.45 µm/sec
µ = 3.37 +/- 0.04 µm/sec
Md = 3.21 µm/sec
µ = 3.21 +/- 0.05 µm/sec
Md = 2.88 µm/sec
µ = 2.87 +/- 0.06 µm/sec
Md = 2.18 µm/sec
µ = 2.23 +/- 0.05 µm/sec
Md = 2.16 µm/sec
µ = 2.19 +/- 0.04 µm/sec
Md = 2.36 µm/sec
µ = 2.34 +/- 0.03 µm/sec
Velocity (µm/sec)
B Pauses
Md = 3.0 per 100 µm
µ = 4.9 +/- 0.3 per 100 µm
Md = 4.1 per 100 µm
µ = 6.7 +/- 0.4 per 100 µm
Md = 2.8 per 100 µm
µ = 7.6 +/- 0.7 per 100 µm
Md = 15.3 per 100 µm
µ = 17.0 +/- 0.7 per 100 µm
Md = 12.7 per 100 µm
µ = 14.3 +/- 0.5 per 100 µm
Md = 12.2 per 100 µm
µ = 14.3 +/- 0.5 per 100 µm
Pauses/100 µm
C Reversals
Anterograde
Retrograde
Direction reversals/100 µm
D
Net reversals per vesicle
Syp
LAMP1
NPY

Figure S1. Supplemental data with quantification of transport parameters for Syp, LAMP1, and NPY-positive vesicles. Related to Figure 1.

A) Velocity, (B) number of pauses and (C) number of transport direction reversals of anterograde- and retrograde-moving Syp-, LAMP1- and NPY-positive vesicles. Across all vesicle populations, anterograde vesicles were faster and paused less often than retrograde-moving vesicles. Vesicles moving in the retrograde direction were observed to change direction more frequently than anterograde-moving vesicles. Generally, however, the reversals were intermittent and the vesicles would reverse back to the original direction, resulting in a net reversal per vesicle very close to 0 as seen in (D). (Syp: 445 anterograde- and 224 retrograde-moving vesicles, from 6 axons from 3 independent cultures; LAMP1: 396 anterograde- and 313 retrograde-moving vesicles, from 10 axons from 4 independent cultures; NPY: 282 anterograde- and 348 retrograde-moving vesicles, from 8 axons from 4 independent cultures).

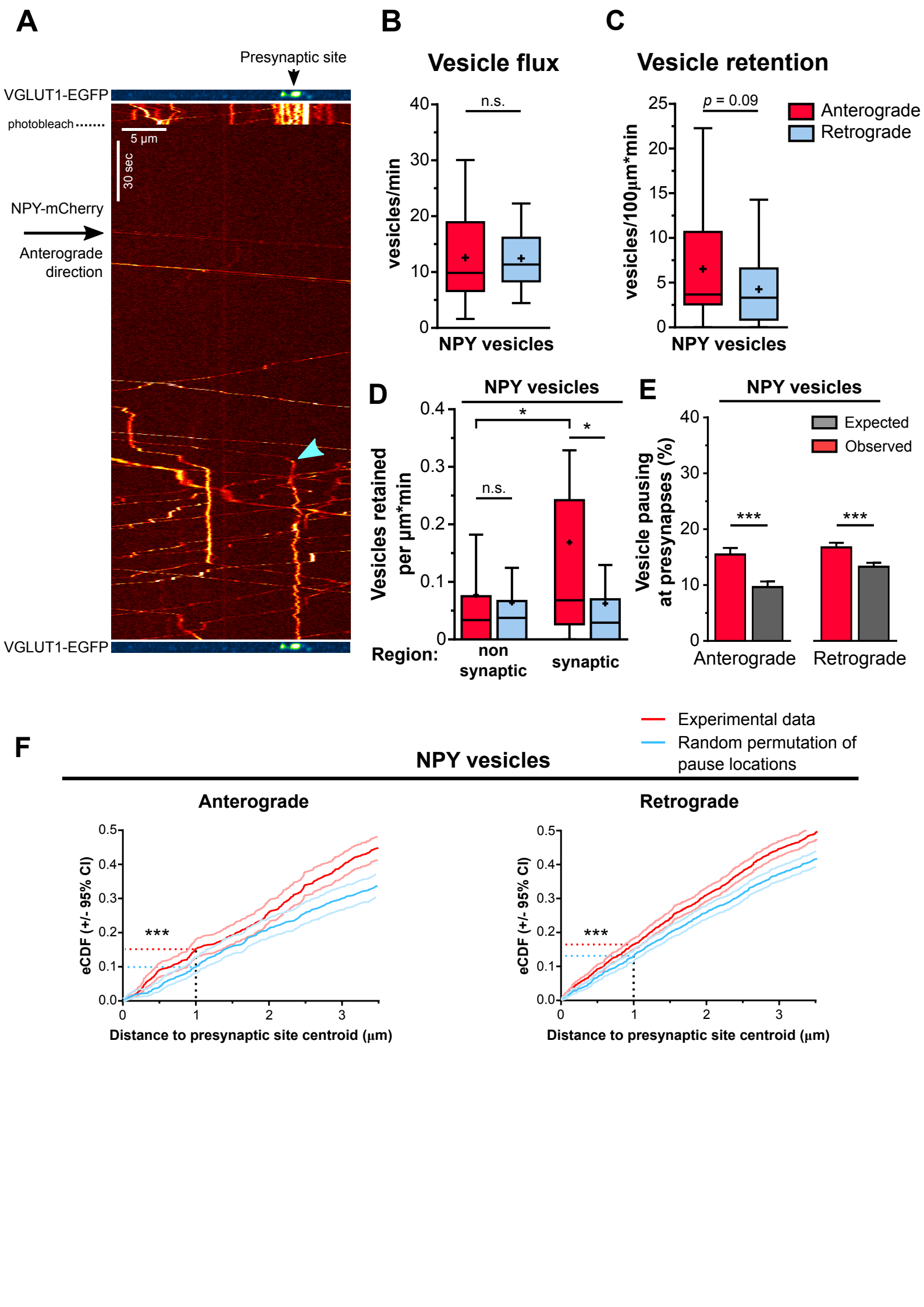
A
Presynaptic site
VGLUT1-EGFP
photobleach
5 µm
30 sec
NPY-mCherry
Anterograde direction
VGLUT1-EGFP
B
Vesicle flux
n.s.
vesicles/min
NPY vesicles
C
Vesicle retention
p = 0.09
Anterograde
Retrograde
vesicles/100µm*min
NPY vesicles
D
NPY vesicles
Vesicles retained per µm*min
n.s.
*
*
Region:
non synaptic
synaptic
E
NPY vesicles
Expected
Observed
Vesicle pausing at presynapses (%)
***
***
Anterograde
Retrograde
F
NPY vesicles
Experimental data
Random permutation of pause locations
Anterograde
Retrograde
eCDF (+/- 95% CI)
***
***
Distance to presynaptic site centroid (µm)
Distance to presynaptic site centroid (µm)

Figure S2. Supplemental data on the flux, pausing, and retention of NPY-positive vesicles. Related to Figure 1.

A) Motility patterns of NPY-positive vesicles along an axonal section of a NPY-mCherry expressing neuron. Upper panel: still showing VGLUT1-EGFP clusters; lower panels: kymograph depicting the motility patterns of NPY-positive vesicles. The axonal section was photobleached to allow the clear visualization and tracking of the motile fraction of NPY-positive vesicles. The cyan arrowhead points to a retention event. B) Flux and retention (C) of anterograde- and retrograde-moving NPY-positive vesicles along axonal sections (n=26 axons from 4 independent cultures; n.s., not significant ($p>0.05$); paired t-test in (B) and Wilcoxon's signed-rank test in (C)). D) Retention of anterograde- and retrograde-moving NPY-positive vesicles at synaptic and non-synaptic regions along the axon (n=34 synaptic and 42 non-synaptic regions from 11 axons from 3 independent cultures; *$p<0.05$; 2-way ANOVA with Sidak's post-hoc test). E) Relative frequency of anterograde- and retrograde-moving NPY vesicle pauses within 1 μm of presynapse centroid. Gray bars represent the expected frequency if vesicles were to pause randomly along the analyzed axonal sections, while red bars represent the observed experimental data. F) Panels show the empirical cumulative distribution functions (eCDFs) related to E) (NPY: 757 pauses in the anterograde direction, 1856 pauses in the retrograde direction and 31 presynaptic sites observed in 7 axons from 3 independent cultures; average±SEM spacing between presynapses = 16.7±2.0 μm).

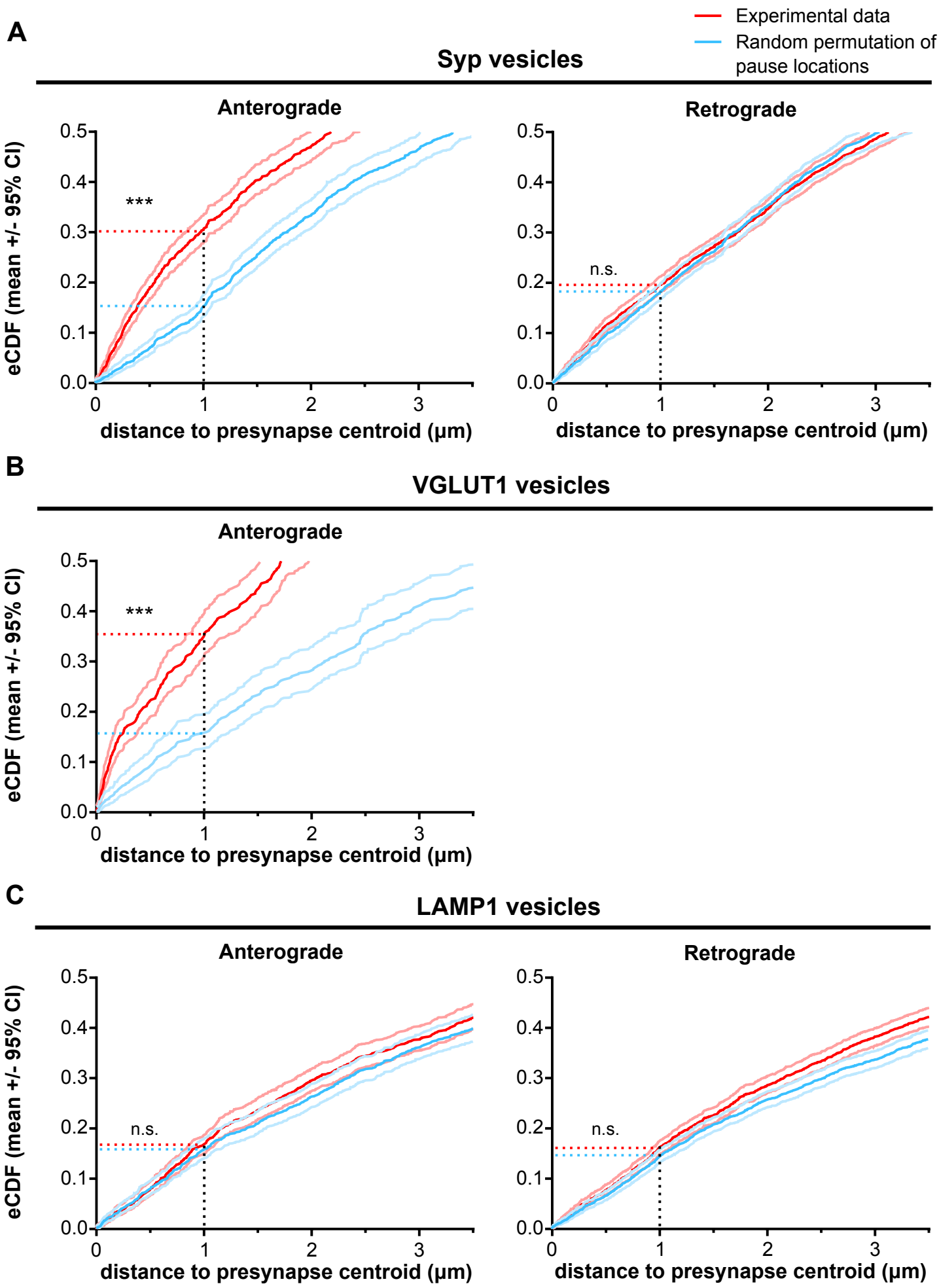
A
Syp vesicles
Experimental data
Random permutation of pause locations
Anterograde
Retrograde
eCDF (mean +/- 95% CI)
***
n.s.
distance to presynapse centroid (µm)
B
VGLUT1 vesicles
Anterograde
***
distance to presynapse centroid (µm)
C
LAMP1 vesicles
Anterograde
Retrograde
n.s.
n.s.
distance to presynapse centroid (µm)
distance to presynapse centroid (µm)

Figure S3. Supplemental data on the nearest presynapse distance of Syp, VGLUT1, and LAMP1 pauses. Related to Figure 1.

Empirical cumulative distribution functions (eCDFs) for the nearest presynapse distance of anterograde- and retrograde-moving Syp (A), VGLUT1 (B) and LAMP1 (C) vesicle pauses. The light red and blue lines represent the upper and lower 95% confidence intervals (CI) for each population (see Materials and Methods for details).

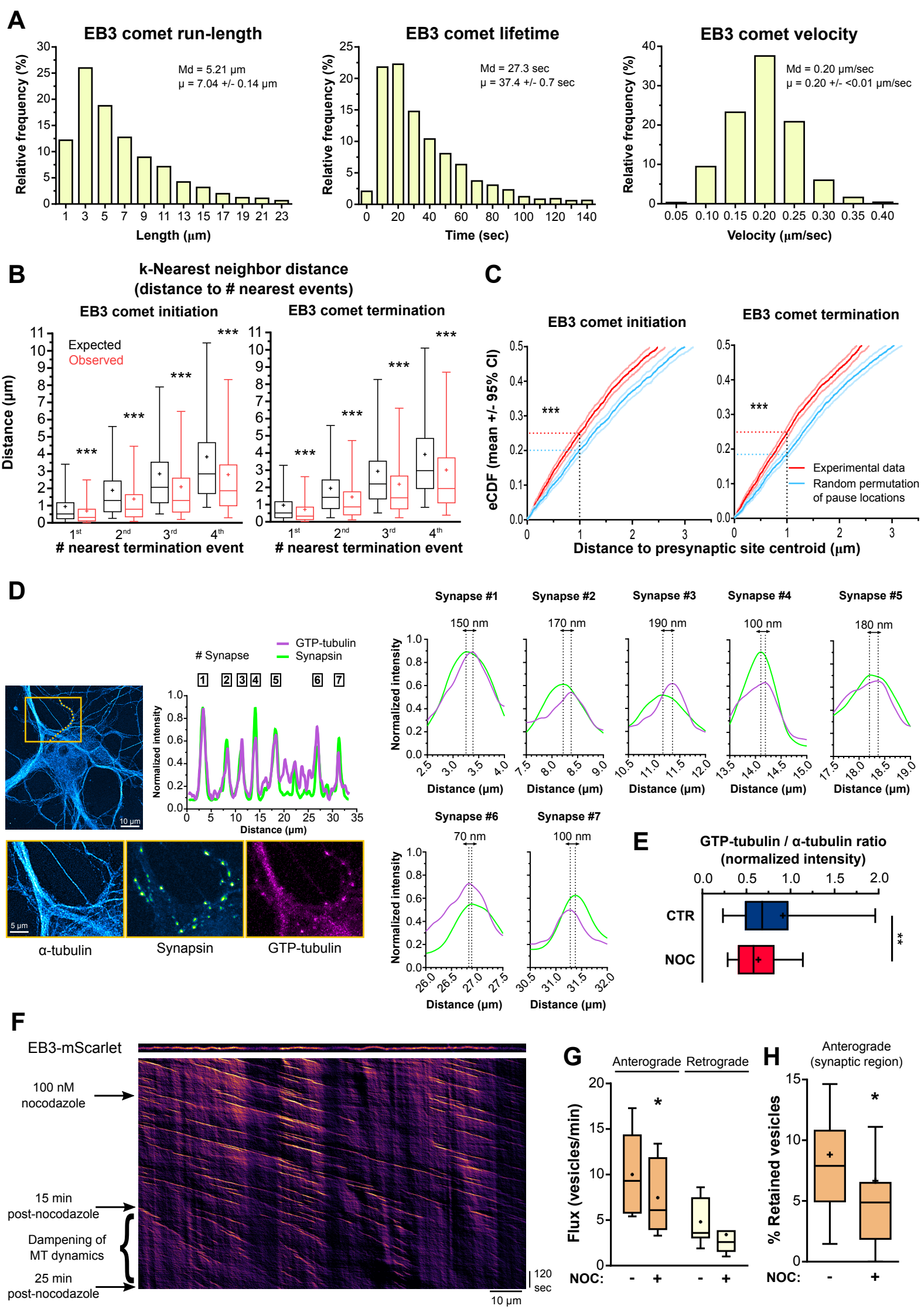
A
EB3 comet run-length
Relative frequency (%)
Md = 5.21 µm
µ = 7.04 +/- 0.14 µm
Length (µm)
EB3 comet lifetime
Md = 27.3 sec
µ = 37.4 +/- 0.7 sec
Time (sec)
EB3 comet velocity
Md = 0.20 µm/sec
µ = 0.20 +/- <0.01 µm/sec
Velocity (µm/sec)
B
k-Nearest neighbor distance
(distance to # nearest events)
EB3 comet initiation
EB3 comet termination
Distance (µm)
Expected
Observed
nearest termination event
C
EB3 comet initiation
EB3 comet termination
eCDF (mean +/- 95% CI)
Experimental data
Random permutation
of pause locations
Distance to presynaptic site centroid (µm)
D
Synapse #1
Synapse #2
Synapse #3
Synapse #4
Synapse #5
Synapse #6
Synapse #7
150 nm
170 nm
190 nm
100 nm
180 nm
70 nm
100 nm
Normalized intensity
Distance (µm)
Synapse
GTP-tubulin
Synapsin
10 µm
5 µm
α-tubulin
Synapsin
GTP-tubulin
E
GTP-tubulin / α-tubulin ratio
(normalized intensity)
CTR
NOC
F
EB3-mScarlet
100 nM
nocodazole
15 min
post-nocodazole
Dampening of
MT dynamics
25 min
post-nocodazole
120
sec
10 µm
G
Anterograde
Retrograde
Flux (vesicles/min)
NOC:
H
Anterograde
(synaptic region)
% Retained vesicles
NOC:

Figure S4. Supplemental data on the enrichment of dynamic microtubules at presynaptic sites. Related to Figure 2.

A) EB3 comet run-length, lifetime and velocity. (n=2560 EB3 comets from 57 axons from 5 independent cultures) B) k-nearest neighbor analysis of EB3 comet initiation and termination events. Distance to the #-nearest neighbors was determined (in red) and compared to the average distance to the #-nearest neighbor of a population in which the initiation and termination events were computationally distributed along the axonal section in a random fashion (in black). C) eCDFs of the nearest presynapse distance of EB3 comet initiation and termination events. Light red and blue lines represent the upper and lower 95% confidence intervals (CI) for each population. (n=3211 EB3 comet initiation events, 3169 EB3 comet termination events and 554 presynaptic sites observed in 57 axons from 5 independent cultures; average ± SEM spacing between presynapses = 14.1 ± 1.4 μm). D) STED microscopy reveals that synapsin clusters and GTP-microtubules are 70-190 nm apart. This distance is in good agreement with previous reports showing that over 90% of active zones in neuromuscular junctions are within 200 nm of a microtubule filament [S13]. E) As a control, the same assay was performed in neurons treated with low dose nocodazole and a significant decrease in GTP-tubulin enrichment at presynaptic sites was observed. F) Upper panel depicts EB3-mScarlet signal along an axonal section. Lower panel is a kymograph obtained from a movie recorded on the same axonal section, depicting EB3 comet and microtubule dynamics before and after the addition of 100 nM nocodazole. Dampening of microtubule dynamics could be detected 15 minutes after nocodazole addition and was prominent after 25 minutes. Detection of the earliest time point in which microtubule dynamics are dampened is important to avoid secondary effects subsequent of microtubule stabilization. G) 30 min 100 nM NOC treatment slightly reduces the anterograde and retrograde flux of SVPs (n = 7 axons from 3 independent cultures; *p<0.05; two-way ANOVA with Sidak's post-hoc test). H) Despite the reduction of SVP anterograde flux after low-dose nocodazole treatment, the fraction of vesicles retained at synapses is also decreased (n=25 synaptic regions from 7 axons from 3 independent cultures; *p<0.05; Wilcoxon signed-rank test).

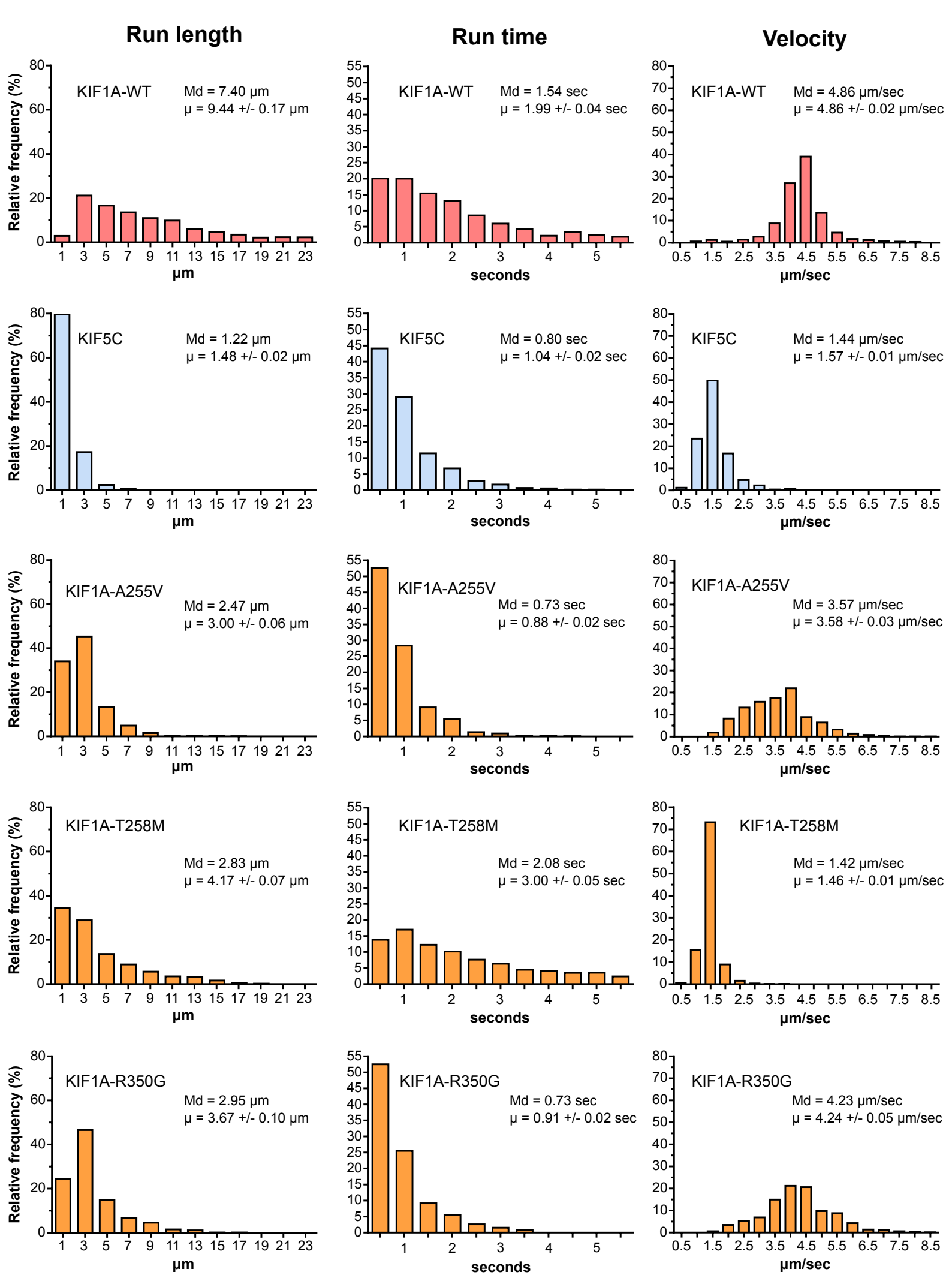
Run length
Run time
Velocity
Relative frequency (%)
KIF1A-WT
Md = 7.40 µm
µ = 9.44 +/- 0.17 µm
Md = 1.54 sec
µ = 1.99 +/- 0.04 sec
Md = 4.86 µm/sec
µ = 4.86 +/- 0.02 µm/sec
KIF5C
Md = 1.22 µm
µ = 1.48 +/- 0.02 µm
Md = 0.80 sec
µ = 1.04 +/- 0.02 sec
Md = 1.44 µm/sec
µ = 1.57 +/- 0.01 µm/sec
KIF1A-A255V
Md = 2.47 µm
µ = 3.00 +/- 0.06 µm
Md = 0.73 sec
µ = 0.88 +/- 0.02 sec
Md = 3.57 µm/sec
µ = 3.58 +/- 0.03 µm/sec
KIF1A-T258M
Md = 2.83 µm
µ = 4.17 +/- 0.07 µm
Md = 2.08 sec
µ = 3.00 +/- 0.05 sec
Md = 1.42 µm/sec
µ = 1.46 +/- 0.01 µm/sec
KIF1A-R350G
Md = 2.95 µm
µ = 3.67 +/- 0.10 µm
Md = 0.73 sec
µ = 0.91 +/- 0.02 sec
Md = 4.23 µm/sec
µ = 4.24 +/- 0.05 µm/sec
µm
seconds
µm/sec

Figure S5. Supplemental data with the quantification of *in vitro* motility parameters of KIF1A-WT, KIF1A mutants, and KIF5C. Related to Figure 3 and 5.

Run-length, run-time and velocity histograms of TMR-labeled KIF1A-WT(1-393)-LZ-HaloTag (n=1841 runs), KIF1A-A255V(1-393)-LZ-HaloTag (n=1044 runs), KIF1A-T258M(1-393)-LZ-HaloTag (n=2344 runs), KIF1A-R350G(1-393)-LZ-HaloTag (n=655 runs), and KIF5C(1-560)-HaloTag (n=1992 runs).

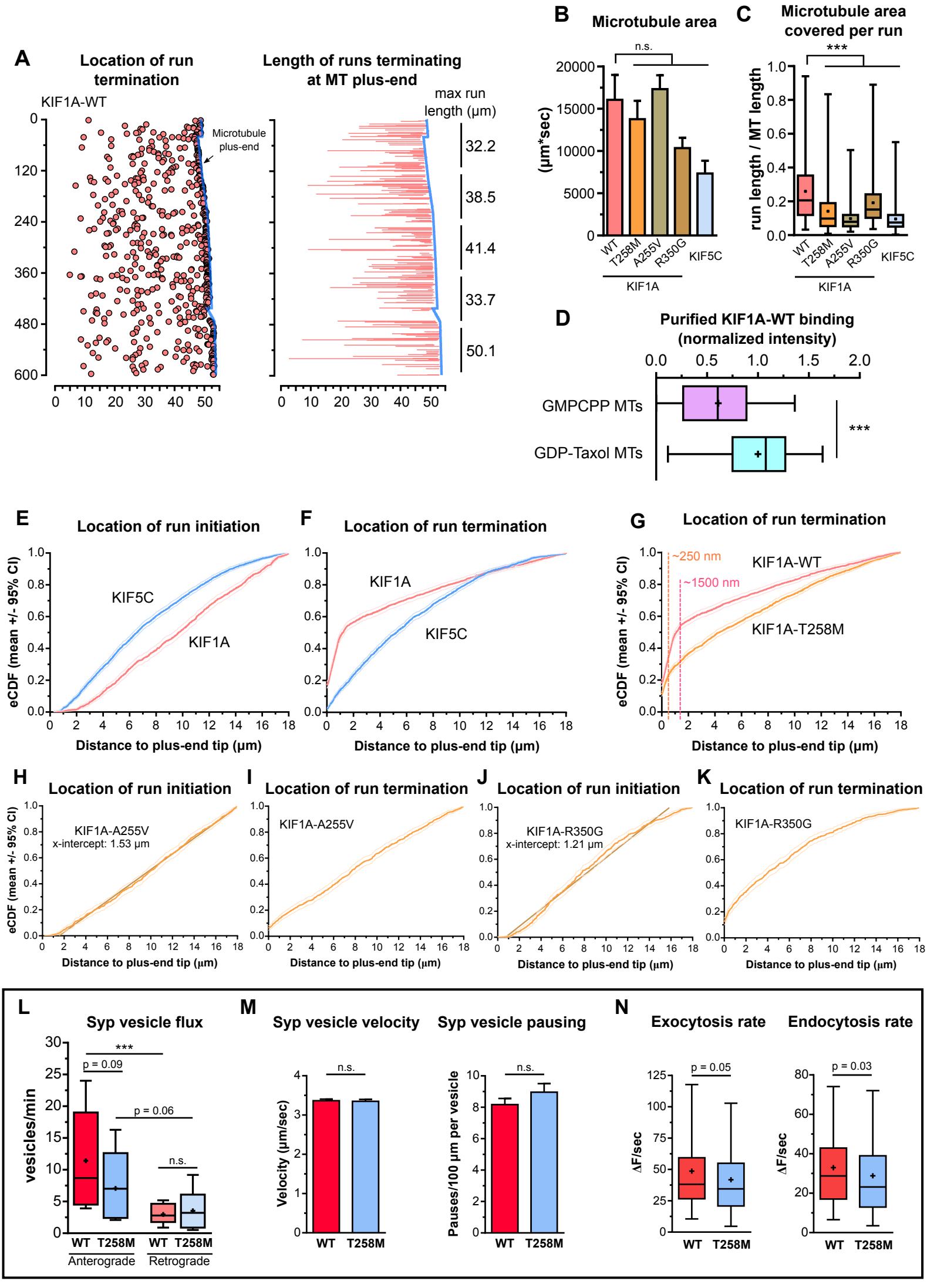
A
Location of run termination
KIF1A-WT
Microtubule plus-end
Length of runs terminating at MT plus-end
max run length (μm)
32.2
38.5
41.4
33.7
50.1
B
Microtubule area
n.s.
(μm*sec)
WT
T258M
A255V
R350G
KIF5C
KIF1A
C
Microtubule area covered per run
***
run length / MT length
D
Purified KIF1A-WT binding (normalized intensity)
GMPCPP MTs
GDP-Taxol MTs
***
E
Location of run initiation
KIF5C
KIF1A
eCDF (mean +/- 95% CI)
Distance to plus-end tip (μm)
F
Location of run termination
G
Location of run termination
~250 nm
~1500 nm
KIF1A-WT
KIF1A-T258M
H
Location of run initiation
KIF1A-A255V
x-intercept: 1.53 μm
I
Location of run termination
J
Location of run initiation
KIF1A-R350G
x-intercept: 1.21 μm
K
Location of run termination
L
Syp vesicle flux
vesicles/min
p = 0.09
p = 0.06
Anterograde
Retrograde
M
Syp vesicle velocity
Velocity (μm/sec)
Syp vesicle pausing
Pauses/100 μm per vesicle
N
Exocytosis rate
ΔF/sec
p = 0.05
Endocytosis rate
p = 0.03

Figure S6. Supplemental data on KIF1A binding and motility behavior *in vitro* and the effects of the full length KIF1A-T258M mutant on synaptic vesicle flux, motility, release and endocytosis in hippocampal neurons. Related to Figure 3, 5, and 6.

A) KIF1A-WT run termination locations on a long dynamic microtubule (~55 μm). Red lines represent the length of KIF1A runs that terminated at the plus-end (dark blue line) of the microtubule. The numbers refer to the maximum KIF1A-WT run-length observed in 120 seconds periods over 10 minutes. B) Average microtubule area of the microtubules in our analysis (KIF1A-WT n=6; KIF1A-A255V n=4; KIF1A-T258M n=5; KIF1A-R350G n=4; KIF5C-WT n=4 microtubule; n.s., non-significant; Kruskal-Wallis with Dunn's post-hoc test). Because motility parameters were obtained in dynamic microtubules, and these can change length throughout the course of imaging, it is important that measurements are performed using microtubules with similar areas (integration of the microtubule length over the movie time course). Microtubule area in the KIF5C was smaller, but with an average run-length of 1.48 μm, this was not a limitation for the accurate depiction of KIF5C motility behavior on dynamic microtubules. C) Microtubule area covered per run (ratio of each run-length by the length of the microtubule at that point in time). (KIF1A-WT n=1841; KIF1A-A255V n=1044; KIF1A-T258M n=2344; KIF1A-R350G n=655; KIF5C-WT n=1992 runs; ***p<0.0001; Kruskal-Wallis with Dunn's post-hoc test). D) Quantification of purified TMR-labeled KIF1A (1-393)-LZ-HaloTag binding to GMPCPP- and GDP-taxol stabilized microtubules in the presence of AMP-PNP. Units are background-subtracted TMR fluorescence units normalized to the to the average KIF1A binding intensity to GDP-taxol-stabilized microtubules. (n=74-300 microtubules per condition; ***p<0.0001; Mann-Whitney U test). E) eCDF showing the location of KIF1A (red) and KIF5C (blue) run initiation and (F) termination, respective to the microtubule plus-end. (Light blue and red lines represent the 95% confidence intervals; KIF1A, n=1841 from 6 microtubules; KIF5C, n=1992 from 4 microtubules). G) eCDF showing the location of KIF1A-WT (red) and KIF1A-T258M (orange) run termination, respective to the microtubule plus-end. Values indicate where motor detachment probability becomes exponential. H) eCDF showing the location of KIF1A-WT (red) and KIF1A-A255V (orange) run initiation, respective to the microtubule plus-end. I) eCDF showing the location of KIF1A-WT (red) and KIF1A-A255V (orange) run termination, respective to the microtubule plus-end (KIF1A-A255V: n=1044

from 4 microtubules). J) eCDF showing the location of KIF1A-WT (red) and KIF1A-R350G (orange) run initiation, respective to the microtubule plus-end. K) eCDF showing the location of KIF1A-WT (red) and KIF1A-R350G (orange) run termination, respective to the microtubule plus-end (KIF1A-R350G: n=655 from 4 microtubules). L) Syp vesicle flux in 14DIV hippocampal neurons expressing full-length KIF1A-WT-GFP or full-length KIF1A-T258M-GFP (n = 9 – 11 axons from 2-3 independent cultures; n.s., non-significant, ***p<0.001; two-way ANOVA with Sidak's post-hoc test). M) Syp vesicle velocity and pausing frequency in 14DIV hippocampal neurons expressing full-length KIF1A-WT-GFP or full-length KIF1A-T258M-GFP (n = 317- 412 vesicles from 5-6 axonal sections from 2-3 independent cultures; n.s., non-significant; Mann-Whitney U test). N) Exocytosis and endocytosis rates of VGLUT1-pHluorin vesicles (n = 236-245 presynaptic sites from 3 independent cultures; Mann-Whitney U test).

Table S1. Biophysical proprieties, clinical symptoms and original references that identified each KIF1A disease mutant. Related to Figure 5.

Mutation (type)	Microtubule Binding*	Processive Motility	Clinical Phenotype	References
c.38G>A, p.R13H (Dominant, de novo)	No	N/A	Autism spectrum disorder, spastic paraplegia and axonal neuropathy	[S1]
c.173C>T, p.S58L (Dominant, de novo)	No	N/A	Language impairment, intellectual disability, ataxia, cerebellar atrophy, spastic paraplegia, neuropathy	[S2]
c.296C>T, p.T99M (Dominant, de novo)	Yes (28.46)	No	Language impairment, intellectual disability, microcephaly, ataxia, spastic paraplegia, epilepsy, cerebellar, cerebral and optic nerve atrophy	[S2-S6]
c.305G>A, p.G102D (Dominant, de novo)	No	N/A	Intellectual disability, spastic paraplegia, cerebellar atrophy and neuropathy	[S2]
c.430G>T, p.V144F (Dominant, de novo)	Yes (25.66)	No	Language impairment, intellectual disability, spastic paraplegia, neuropathy and optic nerve atrophy	[S2]
c.444G>T. p.E148D (Dominant, de novo)	Yes (weakly)	N/A	Intellectual disability, lower limb spasticity, upper limp clumsiness, cerebellar atrophy, visual disturbances	[S7]
c.499C>T, p.R167C (Dominant, de novo)	No	N/A	Intellectual disability, spastic paraplegia, neuropathy, urinary symptoms	[S2, S8]
c.604G>C, p.A202P (Dominant, de novo)	No	N/A	Language impairment, intellectual disability, microcephaly, mixed tone spasticity, cerebral and optic nerve atrophy	[S2]
c.643A>C, p.S215R (Dominant, de novo)	Yes (1.57)	No	Language impairment, intellectual disability, microcephaly, epilepsy, spasticity paraplegia, neuropathy, cerebellar, cerebral and optic atrophy	[S2, S9]
c.647G>C, p.R216P (Dominant, de novo)	No	N/A	Language impairment, intellectual disability, spastic paraplegia, cerebellar and optic nerve atrophy	[S2]

c.746T>A, p.L249Q (Dominant, de novo)	No	N/A	Intellectual disability, spastic paraplegia, optic nerve atrophy	[S2]
c.757G>A, p.E253K (Dominant, de novo)	Yes (3.90)	No	Language impairment, intellectual disability, microcephaly, spastic paraplegia, neuropathy, cerebellar, cerebral and optic nerve atrophy, early death	[S2, S5]
c.760C>T, p.R254W (Dominant, de novo)	No	N/A	Intellectual disability, lower limb spasticity, upper limb clumsiness, neuropathy, cerebellar atrophy, visual disturbances	[S7]
c.761G>A, p.R254Q (Dominant, de novo)	Yes (weakly)	N/A	Intellectual disability, lower limb spasticity, cerebellar atrophy	[S7]
c.765C>T, p.A255V (Recessive, inherited)	Yes (1.71)	Yes (minus-end directed steps observed)	Spastic paraplegia, neuropathy	[S10, S11]
c.773C>T, p.T258M (Dominant, inherited)	Yes (1.06)	Yes	Language impairment, intellectual disability, microcephaly, epilepsy, spastic paraplegia, neuropathy, scoliosis, thinning of the corpus callosum, optic nerve atrophy	[S12]
c.946C>T, p.R316W (Dominant, de novo)	No	N/A	Language impairment, intellectual disability, microcephaly, epilepsy, ataxia, spastic paraplegia, cerebellar, cerebral and optic nerve atrophy	[S2, S5, S7]
c.1048C>G, p.R350G (Recessive, inherited)	Yes (2.08)	Yes	Spastic paraplegia, ataxia, neuropathy, cerebellar atrophy	[S11]

* Numbers refer to the GDP-taxol- vs. GMPCPP-stabilized microtubules binding ratio.

Supplemental References

S1. Tomaselli, P.J., Rossor, A.M., Horga, A., Laura, M., Blake, J.C., Houlden, H., and Reilly, M.M. (2017). A de novo dominant mutation in KIF1A associated with axonal neuropathy, spasticity and autism spectrum disorder. Journal of the peripheral nervous system : JPNS *22*, 460-463.

S2. Lee, J.R., Srour, M., Kim, D., Hamdan, F.F., Lim, S.H., Brunel-Guitton, C., Decarie, J.C., Rossignol, E., Mitchell, G.A., Schreiber, A., et al. (2015). De novo mutations in the motor domain of KIF1A cause cognitive impairment, spastic paraparesis, axonal neuropathy, and cerebellar atrophy. Human mutation *36*, 69-78.

S3. Hamdan, F.F., Gauthier, J., Araki, Y., Lin, D.T., Yoshizawa, Y., Higashi, K., Park, A.R., Spiegelman, D., Dobrzeniecka, S., Piton, A., et al. (2011). Excess of de novo deleterious mutations in genes associated with glutamatergic systems in nonsyndromic intellectual disability. American journal of human genetics *88*, 306-316.

S4. Okamoto, N., Miya, F., Tsunoda, T., Yanagihara, K., Kato, M., Saitoh, S., Yamasaki, M., Kanemura, Y., and Kosaki, K. (2014). KIF1A mutation in a patient with progressive neurodegeneration. Journal of human genetics *59*, 639-641.

S5. Esmaeeli Nieh, S., Madou, M.R., Sirajuddin, M., Fregeau, B., McKnight, D., Lexa, K., Strober, J., Spaeth, C., Hallinan, B.E., Smaoui, N., et al. (2015). De novo mutations in KIF1A cause progressive encephalopathy and brain atrophy. Annals of clinical and translational neurology *2*, 623-635.

S6. Langlois, S., Tarailo-Graovac, M., Sayson, B., Drogemoller, B., Swenerton, A., Ross, C.J., Wasserman, W.W., and van Karnebeek, C.D. (2016). De novo dominant variants affecting the motor domain of KIF1A are a cause of PEHO syndrome. European journal of human genetics : EJHG *24*, 949-953.

S7. Ohba, C., Haginoya, K., Osaka, H., Kubota, K., Ishiyama, A., Hiraide, T., Komaki, H., Sasaki, M., Miyatake, S., Nakashima, M., et al. (2015). De novo KIF1A mutations cause intellectual deficit, cerebellar atrophy, lower limb spasticity and visual disturbance. Journal of human genetics *60*, 739-742.

S8. Citterio, A., Arnoldi, A., Panzeri, E., Merlini, L., D'Angelo, M.G., Musumeci, O., Toscano, A., Bondi, A., Martinuzzi, A., Bresolin, N., et al. (2015). Variants in KIF1A gene in dominant and sporadic forms of hereditary spastic paraparesis. Journal of neurology *262*, 2684-2690.

S9. Raffa, L., Matton, M.P., Michaud, J., Rossignol, E., Decarie, J.C., and Ospina, L.H. (2017). Optic nerve hypoplasia in a patient with a de novo KIF1A heterozygous mutation. Canadian journal of ophthalmology. Journal canadien d'ophtalmologie *52*, e169-e171.

S10. Erlich, Y., Edvardson, S., Hodges, E., Zenvirt, S., Thekkat, P., Shaag, A., Dor, T., Hannon, G.J., and Elpeleg, O. (2011). Exome sequencing and disease-network analysis of a single family implicate a mutation in KIF1A in hereditary spastic paraparesis. Genome research *21*, 658-664.

S11. Klebe, S., Lossos, A., Azzedine, H., Mundwiller, E., Sheffer, R., Gaussen, M., Marelli, C., Nawara, M., Carpentier, W., Meyer, V., et al. (2012). KIF1A missense mutations in SPG30, an autosomal recessive spastic paraplegia: distinct phenotypes according to the nature of the mutations. European journal of human genetics : EJHG *20*, 645-649.

S12. Cheon, C.K., Lim, S.H., Kim, Y.M., Kim, D., Lee, N.Y., Yoon, T.S., Kim, N.S., Kim, E., and Lee, J.R. (2017). Autosomal dominant transmission of complicated hereditary spastic paraplegia due to a dominant negative mutation of KIF1A, SPG30 gene. Scientific reports *7*, 12527.

S13. Lepicard, S., Franco, B., de Bock, F., and Parmentier M-L. (2014). A presynaptic role of microtubule-associated protein 1/Futsch in *Drosophila*: regulation of active zone number and neurotransmitter release. Journal of Neuroscience *34*, 6759-6771.